Definition of a general performance map for single stage radial inflow turbines and analysis of the impact of expander performance on the optimal ORC design in on-board waste heat recovery applications.

Marco Manfredi[a], Andrea Spinelli[a], Marco Astolfi[a]

[a]*Politecnico di Milano, Energy Department, , Milano, 20156, , Italy*

Abstract

Small-scale Organic Rankine Cycles (ORCs) represent a promising technology for waste heat recovery (WHR) from internal combustion engines (ICEs) for transport applications, due to their remarkable potential, especially on-board of innovative long-haul trucks. Despite market leader companies have already proved its effectiveness, detailed system design procedures are scarcely available in the open literature and proposed solutions are often more simplified with respect to current industrial state-of-art. The present work describes a methodology to include within the ORC design and optimization procedure an efficiency map of the turbo-expander, retrieved exploiting a reduced-order method developed in-house. The proposed approach allows therefore to design the thermodynamic cycle considering a realistic performance of the expander and to retrieve the best cycle architectures and turbine geometry depending on heat source characteristics and active constraints. First the turbine performance is defined in general terms and investigation of its applicability to different fluids and to expansions characterized by various degrees of non-ideality is provided. Then, the methodology is applied to different WHR applications highlighting for several potential working fluids the impact of adopting turbine performance maps within the cycle optimization procedure rather than assuming constant efficiency values. Results show that the cycle configuration and the main design parameters are strongly affected by the plant size and the working fluid selection, and that the adoption of a turbine performance map is particularly valuable when dealing with small size power plants adopting high density fluids. In particular, the assumption of constant turbine efficiency may lead to the definition of thermodynamic cycles extremely far from the optimal ones (e.g. adoption of supercritical cycles rather than subcritical ones) that in turn can result in unfeasible design of the turboexpander. Moreover, this simplified assumption may also lead to an incorrect comparison between different candidate working fluids lacking in identify those more suitable for a specific plant size. Both those limits can be solved with the adoption of the expander performance map proposed in this work. Final results show that on board WHR ORC can reach an efficiency of at least 20% in a relatively large range of internal combustion engine size. On the contrary, the choice of the best working fluid is affected by engine size and chosen hot source: for small available thermal power the use of complex and flammable hydrocarbons (cyclopentane, cyclohexane, toluene) is the most efficient choice while the use of low GWP non-flammable halogenated hydrocarbons (R1233zd and R245fa) becomes promising only for relatively large available thermal power.

Keywords: Organic Rankine Cycle, On-board WHR, Radial-Inflow Turbines, Reduced-Order Models, Performance Map, Cycle Optimization

1. Introduction

Despite the employment of organic Rankine cycle (ORC) technology for stationary thermal recovery in the power range from 10^{-1} to 10^{1} MW is widely spread [1], economic and technical challenges prevent the penetration of ORCs into automotive and transportation freight sectors [2]. However, they represent a promising solution due to the remarkable recovery potential from internal combustion engines (ICEs), which release a large fraction of the fuel energy at high-temperature through the engine hot exhaust (about 30% of the fuel inlet power) and the EGR system (about 5-10%), and at low-temperature from the charge-air cooler (about 5-10%) and the engine cooling system (about 10-15%) [3]. Despite the large market potential, design methods for onboard small-scale ORCs are not trivial requiring a meaningful working fluid and heat sources selection and an optimal design and performance quantification of the thermodynamic cycle and of the small-scale components in both nominal, part load and transient conditions [4, 5]. For small power applications, volumetric machines are often preferred over turbo-expanders but they are limited by low theoretical efficiencies and constrained by limited volumetric expansion ratios [6, 7, 8], making unfeasible their efficient employment in high-temperature applications. For this reason, radial inflow turbines (RITs) are usually exploited, being characterized by large power density and capability to handle high pressure ratios (PRs) within a single-stage configuration [9].

Despite market leader companies have already proved its effectiveness [10], the design procedures of bottoming ORCs available in the open literature are often more simplified with respect to current industrial state-of-art and usually adopts simplified assumptions relative to the performance of the components. In particular, the quantification of turbine efficiency during the cycle design optimization procedure is of paramount importance because of the large impact on the definition of optimal working fluid and design parameters (e.g. maximum and minimum pressure of the cycle). In the framework of small-scale ORC design for onboard WHR, assuming a constant turbine efficiency may result into misleading optimal cycle configurations having turbine expansion ratios and dimensions non compatible with the assumed turbine efficiency, especially if the number of stages and the rotational speed are constrained by rotodynamic, available space and economic factors. Similarly, a coupled sensitivity analysis on turbine efficiency [11] results ineffective to optimize the ORC design variables, since they are only slightly affected by the specific value of the turbine efficiency. An apparently more reliable and complex iterative procedure, in which the ORC and turbine optimization routines are iteratively alternated [12] turns out to be also inadequate, the turbine efficiency being still constant at each ORC optimization step, despite estimated with a dedicated design tool. A more reliable method would instead integrate the turbine efficiency quantification into the ORC optimization process to account for realistic turboexpander performance as function of the inlet/outlet thermodynamic states at each ORC design iteration step. This is usually achieved through turbine reduced-order (or mean-line) models, capable of providing preliminary sizing and performance evaluation with a limited computational cost. The most rigorous method would require the implementation of a dedicated turboexpander optimization routine within the ORC cycle optimization tool, however this approach implies a non-feasible computational cost (even using mean line models) since several hundreds of turbine mean-line model evaluations should be performed at each ORC design iteration step. Alternatively, a higher-order optimization may be performed by varying concurrently the ORC design parameters and the geometric variables of the turbine model [13]. However, this approach may converge to local minima, due to the different effect of geometric and thermodynamic design variables on the turbine performance and may lead to suboptimal solutions since a low number of turbine and cycle optimized parameters is usually adopted in order to reduce the complexity of the numerical problem. Finally, other studies propose to exploit the turbine design tools to retrieve performance maps as a function of certain cycle-dependent non-dimensional parameters [14, 15, 16, 17].

Differently from most of the available literature that adopts fixed turbine efficiency [11, 12, 4], in this work a maximum efficiency performance map for single-stage radial inflow turbines (RIT) is integrated in the cycle optimization procedure. This map reports the maximum RIT total-to-static efficiency η_{TS} as function of turbine Size Parameter (SP) and isentropic Volume ratio (Vr), since their definition includes the effects of fluid properties (complexity and non-ideality) and they were identified as the most adequate independent parameters from previous studies on ORC axial and radial turbines [18, 14, 15, 16, 19]. In addition, the performance map proposed in this work was obtained performing expander optimizations, aiming at maximizing η_{TS}, for a discrete number of SP and Vr values representing a substantial improvement with respect to the approach suggested by [17], in which the map was retrieved by means of a scaling procedure applied to the results published by [14]. Specifically, in the proposed method the RIT optimization was carried out exploiting an in-house reduced-order model, whose details are thoroughly reported in [20], which adopts 10 design variables, including most of geometrical parameters and rotor rotational speed, and adopting several constraints, which have been included to obtain feasible RIT geometries. This represents a further improvement with respect to the approach of [16], where maps were obtained exploiting a bivariate optimization procedure based on specific speed and velocity ratio. Therefore, the map here reported defines an ultimate upper bound for the RIT efficiency. Finally, since high-temperature small-power applications are considered, the ranges of Vr and SP investigated are wider than those reported in [16] and shifted towards higher Vr and lower SP, requiring to analyze converging-diverging nozzles in choking conditions, while previous studies only investigated converging-nozzle architectures [14, 16].

2. Numerical tools description

Two numerical models have been developed and integrated for this study: the first one deals with the ORC cycle optimization while the second one concerns the design and optimization of single-stage radial inflow turbines and will be used for the development of the map of maximum turbine efficiency. Both models are implemented in Python and adopt CoolProp [21] for the calculation of fluid thermodynamic properties recalling the NIST REFPROP backend [22].

2.1. ORC Numerical tool description and assumptions

The numerical code developed for on-board WHR with ORC power systems implements several features that make it a flexible tool for system optimization and technoeconomic analysis. However, the potential of the code is not fully exploited in this work according to the scope of the paper which is to investigate the strong link between turbine performance and cycle design rather than determine optimal cycle architecture from technoeconomic perspective. Despite the numerical code can analyze ORC systems integrated with multiple thermal power inputs, a single heat source is considered, namely the engine exhaust. MAN D2676 [23], with 316 kW nominal brake power output at 1800 rpm, is selected as reference engine and exhaust reference thermodynamic conditions are obtained at 50% of the engine load. In this condition, the hot exhaust stream, modelled as ideal gas with constant specific heat (1.035 kJ/kgK), has mass flow rate equal to 0.2 kg/s and temperature at the primary heat exchanger (PRHE) inlet equal to 351°C. The developed numerical code can deal with any fluid available in RefProp database. A single pressure level cycle is selected in both subcritical and supercritical configurations, being saturated cycles considered as a subclass of subcritical ones with no vapor superheating, and the employment of the recuperator can be optionally activated. The ORC optimization procedure aims at minimize/maximize a selected objective function by varying a certain number of design variables. In this research work, the selected objective function is the ORC plant system efficiency, which is proportional to the net power output and can be expressed as the product of cycle thermodynamic efficiency and heat recovery factor, as reported in Equation 1. However, the model can be easily adapted for more complex analyses as technoeconomic (minimization of system specific cost or levelized cost of electricity) and multi-objective optimizations.

$$ObjFunc.: \quad W_{el} = W_{gen} - W_{pump} - W_{fan}\,, \tag{1a}$$

$$ObjFunc.: \quad \eta_{system} = \eta_{cycle}\chi_{recovery} = \frac{W_{el}}{Q_{in}}\frac{Q_{in}}{Q_{in,max}} \tag{1b}$$

ΔT heat exchangers		Heat exchangers pressure drops	
$\Delta T_{pp,PRHE}$, °C	10	ΔT_{cond}, °C	0.5
$\Delta T_{pp,cond}$, °C	2	ΔP_{desh}, %	0.02
Components efficiency		ΔP_{eco} (sub), bar	0.5
η_{pump}	0.5	ΔT_{eva} (sub), °C	1
η_{turb}	Fixed or Calculated	ΔP_{sh} (sub), bar	0.5
$\eta_{el,mecc,gen}$	0.98	ΔP_{PRHE} (sup), bar	1
$\eta_{el,mecc,pump}$	0.98	ΔP_{rec} (sup), %	0.002
η_{fan}	0.7	ΔP_{air}, mbar	22

Table 1: ORC model assumptions.

Four DVs are selected: (i) condensation temperature, cycle (ii) maximum pressure and (iii) maximum temperature and (iv) recuperator pinch point temperature difference. Table 1 reports all the other plant quantities needed for the complete cycle definition. These values are derived from literature review [24] and are kept constant during the plant optimization procedure independently of the working fluid selected and the maximum/minimum pressure of the cycle. Among them, the turbine efficiency can be set equal to a fixed value or calculated as function of other cycle parameters by means of the performance map described in Section 3.4, in order to have a clear link between cycle DVs and expander performance. Some constraints are considered in the optimization procedure, among which the most limiting are: avoidance of two-phase flow expansion (i.e. vapor quality larger than one at the turbine outlet), and a maximum volume ratio Vr equal to 60 in order to avoid unfeasible single-stage turbine designs. ORC is condensed in a direct dry air-cooled heat exchanger having a design analogous to engine radiator: nominal air ambient temperature is equal to 25°C. A high-rotational speed generator is considered in order to allow for effective turbine efficiency optimizations avoiding the use of gearbox. The optimization routine includes a global gradient-free optimization procedure implementing a self-adaptive Differential Evolution algorithm and a local one exploiting SLSQP, a sequential quadratic programming (SQP) algorithm for nonlinearly constrained gradient-based optimizations.

2.2. RIT reduce-order model description

The comprehensive reduced-order model developed, named RITML, implements several features that make it a flexible tool to carry out a preliminary design of single-stage radial inflow turbines, especially tailored for machines operating with organic fluids and for small-power high-temperature applications. In this section the main features are presented but its detailed description, together with a rigorous validation strategy, may be found in a paper recently published [25].

The mean-line method, i.e. a low-fidelity approach based on the solution of 1D continuity, energy, and momentum equations, alongside loss correlations, includes the design of the nozzle, either of converging or converging-diverging type, the vaneless interspace, the rotor, with either radial or back-swept blades at the inlet, and, eventually, of a downstream conical diffuser. An independent routine for each component is sequentially solved by the code, leading to a flexible and modular design procedure. To properly take into account the loss generation mechanisms across each component, a suitable set of empirical models was selected through a loss sensitivity analysis, whose details can be found in [20] together with the set of loss correlations employed. The mandatory parameters required as inputs by the method to carry out the design are the inlet conditions, namely the total inlet pressure, and temperature, the flow angle at the nozzle inlet, the mass flow rate, and the required pressure ratio. In addition to the inputs, other parameters, also referred to as design variables (DVs), which include several geometrical parameters and the rotor rotational speed, are required to solve the flow field at each turbine station. The method implements a strategy to handle nozzle choking conditions and three different geometries may be contemporary investigated: converging subsonic nozzles, converging ones in chocking conditions with post-expansion, and supersonic converging-diverging geometries. However, the analyses and the turbine design procedures carried out in the present work are limited to converging-diverging nozzle, since the large Vr values involved correspond to high pressure ratios through the machine that in turn lead to supersonic Mach numbers at the stator outlet, for which a converging-diverging nozzle architecture results more efficient. The model retrieves the full turbine geometry, comprehensive of nozzle/rotor blade angles, clearances, blade thicknesses, cascade pitches, chords and openings, evaluates the average flow quantities and thermodynamic state at each turbine section, and estimates its performance, as proved by the extensive validation procedure against the performance data of 7 radial turbines, reported in [20].

DVs	Variation Ranges	DVs	Variation Ranges
ω_s	0.7-1.3	$\beta_{e,PE}$	0.9-1.1
α_3, deg	70-81	$r_{6,hub}$, m	0.006-0.1
$r_{6,hub}/r_{6,sh}$	0.1-0.7	$r_4/r_{6,sh}$	1.15-1.5
r_3/r_4	1.005-1.1	r_1/r_3	1.1-1.5
b_4/D_4	0.03-0.09	L_z/r_4	1.1-1.5

Table 2: Optimization procedure DVs and corresponding variation ranges.

The DVs can be optimized in order to maximize turbine total-to-static efficiency, exploiting an outer algorithm to be coupled with RITML. In particular, the same optimization routine described at the end of Section 2.1 is implemented, which involves both gradient-free global and nonlinearly-constrained gradient-based local optimization procedures. The number and kind of DVs to be included in the optimization problem may be freely set by the user, making the code flexible and suitable for multi-level design strategies. Table 2 lists the parameters considered as DVs for such procedures and the corresponding ranges of variation, which define the design space investigated by the optimization algorithms. In Table 2 the subscripts 3, 4, 6 refer to nozzle outlet, rotor inlet and rotor outlet respectively. $\beta_{e,PE}$ is the post-expansion/post-compression pressure ratio, defined as the ratio between the pressure at the inlet of the semi-bladed region over the one at the nozzle outlet (i.e. at radius r_3), and defines the degree of under-expansion/over-expansion in supersonic nozzles. Several constraints are considered in the present analysis to supervise those parameters which are not directly optimized and to avoid non-physical solutions. It is worthwhile to highlight that the lower limit of each physical dimension of the turbine was constrained to a certain minimum value (e.g. rotor hub radius > 6 mm, rotor axial length > 5 mm, stator heights and rotor inlet height > 2 mm, trailing edge $> 0.15-0.25$ mm for stator and rotor respectively, axial, radial and backplate clearance > 0.1 mm, nozzle radial chord > 5 mm) to ensure the feasibility of the final proposed geometry. Other constraints concern the flow field, such as for example the maximum Mach number at the nozzle outlet (< 2.5), the maximum flow turning within the rotor ($< 120°$), or the maximum relative Mach number at the rotor inelt/outlet (< 1).

3. Preliminary analysis and turbine map definition

3.1. Preliminary considerations on ORC design

The ORC numerical code has been adopted for a preliminary analysis in which several hundreds of cycles are designed considering different constant turbine efficiency values. Hydro-fluoro-olefin R1233zd(E) has been selected as working fluid in this analysis as an environmentally friendly drop-in substitute fluid for R245fa with extremely low ODP, very small GWP, and low safety issues, and therefore widely suggested as a promising candidate for automotive climatization as it is compatible with present and future regulation [26]. The objective of such analyses is to retrieve useful ranges of SP and Vr to set as bounds for the development of the expander maximum efficiency map. Both recuperative ($\Delta T_{pp,rec}$ = 2°C) and non-recuperative cycles are investigated while three turbine efficiency values are adopted, namely 70%, 80% and 90%. The others three design variables defined in Section 2.1 are varied in the following ranges in order to cover the whole design space for the ORC cycle:

- *Cycle maximum pressure*. Both subcritical and supercritical cycles are investigated in the range between 7.4 bar, corresponding to a low evaporating temperature of 85°C, and 107.2 bar, corresponding to 3 times the critical pressure;

- *Cycle condensation temperature*. Minimum value (29°C) corresponds to very small pinch point temperature difference and wide heat transfer area condenser and implies a minimum pressure of 1.5 bar, compatible with the avoidance of non-condensable gases leakage. Maximum value (80°C) is selected in order to investigate also supercritical cycles with non-excessive pressure ratio;

- *Turbine inlet temperature*. Minimum value coincides with saturated condition for medium-low evaporation temperature subcritical cycles while it is affected by the constraint of single-phase flow expansion for high pressure subcritical and supercritical cycles. Maximum value is defined by fluid thermal stability temperature.

Optimal design of the six cycles is reported in Table 3. It is of interest to note that all the optimal configurations are supercritical, adopt a similar condensation temperature, which is higher than the lower bound, and push

Cycle	Non Recuperative			Recuperative ($\Delta T_{pp,rec}$=2°C)		
η_{turb}	70%	80%	90 %	70%	80%	90 %
Case	A	B	C	D	E	F
T_{cond}, °C	38.5	37.7	37.2	36.6	36.1	35.4
P_{max}, bar	57	60.2	62.7	53.6	56.0	58.7
T_{max}, °C	240	240	240	240	240	240
η_{sys}	12.6	15.0	17.4	15.0	17.8	20.6
W_{el}, kW	6.8	8.1	9.4	8.1	9.6	11.1
$\dot{m}_{ORC}$, g/s	169.6	171.4	172.9	201.0	201.6	201.6
SP, mm	8.2	8.3	8.4	9.1	9.2	9.2
Vr	30.7	33.7	36.1	29.0	31.8	34.2

Table 3: Optimal cycle results for the six investigated plants in the preliminary analysis with R1233zd(E).

the turbine inlet temperature up to the maximum value. Optimal cycle efficiency is strongly affected by turbine efficiency while working fluid mass flow rate is mainly affected by the presence of the recuperator. These results also prove that a sensitivity analysis on turbine efficiency as proposed by [11] is not the correct approach to optimize an ORC power plant: optimal cycle design parameters are slightly affected by turbine assumed efficiency and the higher is the efficiency the higher is the turbine Vr, which is unrealistic when a single-stage turbine is adopted. Figure 1.a depicts the maximum system efficiency as function of condensation temperature and maximum pressure always at the optimal cycle maximum temperature for a non-recuperative cycle with 80% turbine efficiency (case B of Table 3). Contours of iso-SP and iso-Vr are also reported together with the optimal design point (red dot). It is possible to underline that the region of maximum efficiency is extremely wide and extends up to very high cycle maximum pressure and pretty high condensation temperatures, corresponding to intermediate values of both SP ($0.007 < \text{SP} < 0.009$) and Vr spanning in a wide range ($15 < \text{Vr} < 55$). Figure 1.b depicts the system efficiency as function of turbine SP and Vr for case B and concurrently delimits the ranges of SP and Vr for the other cases, reporting the corresponding envelopes (colored lines). Finally, marker locations define the optimal solution for each case reported in Table 3. Results clearly highlight that the envelops of Vr and SP are quite

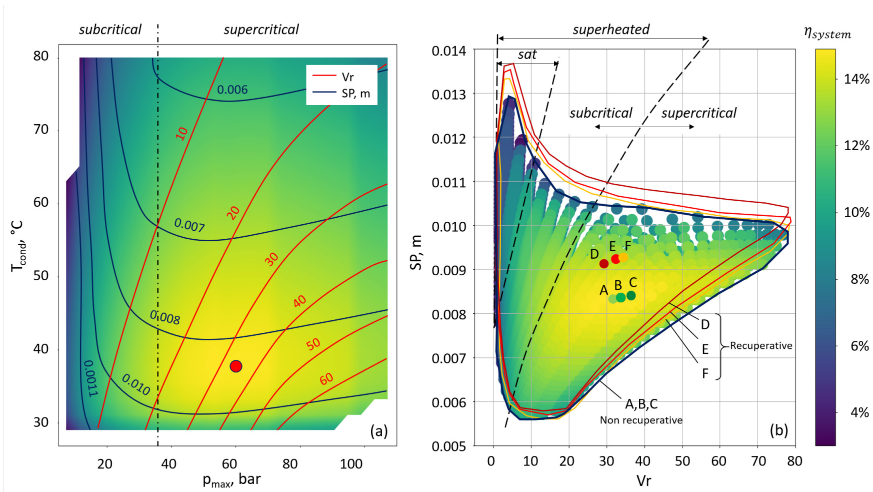

Figure 1: Graphical results for Case B: (a) maximum cycle efficiency, SP and Vr isolines as function of cycle maximum pressure and condensation temperature at optimal turbine inlet temperature (b) maximum cycle efficiency reported on turbine SP and Vr map, plus envelope of SP and Vr for the different investigated cycles (lines) and location of optimal designs (markers).

overlapped and they are thus not particularly affected by both the adoption of recuperator and the actual value of turbine efficiency. This suggests that the choice of Vr and SP ranges based on the envelopes reported in Figure 1.b is appropriate and would lead to a turbine performance map definition that can be used during the cycle optimization independently of the cycle architecture.

3.2. RIT efficiency sensitivity analysis: effects of compressibility factor Z

In order to check the consistency of adopting SP and Vr as independent parameters for the turbine analyses, four RITs working with R1233zd(E) and having the same SP (0.011 m) and Vr (14) but characterized by different expansion inlet and outlet conditions and compressibility factors are optimized adopting RITML code, as summarized in Table 4. Turbine X expands from saturated conditions, turbine Y is representative of a superheated subcritical cycle while turbines K and W expand from supercritical region, leading to inlet compressibility factor values ranging from 0.41 to 0.82. It is possible to note that not only the non-dimensional parameters but also the physical geometric dimensions of the four turbines are rather similar, all of them being characterized by the same SP. Although the rotational speed is

Parameter	Turbine X	Turbine Y	Turbine K	Turbine W
T_{in} - P_{in}, °C - bar	130.3, 19.2	205.9, 22.8	213.4, 45	192.5, 50
T_{out} - P_{out} , °C - bar	46.6, 1.6	121.9, 1.6	116.7, 3.8	84.3, 5.8
m_{ORC}, g/s	219.9	205.1	471.3	681.9
Z_{in} - Z_{out}	0.66, 0.95	0.82, 0.98	0.63, 0.94	0.41, 0.87
η_{turb}, %	90.1	89.7	90.5	91
Nozzle				
D_{in} - D_{out}, mm	44.4, 34.4	45.2, 35.2	44.3, 34.3	44.3, 34.3
h_{in} -h_{out}, mm	2.6, 2.6	2.7, 2.7	2.7, 2.7	2.9, 2.9
Rotor				
ω_s - ω, kRPM	0.97, 96.8	0.94, 112	0.97, 105	0.97, 85
D_{in} - D_{out}, mm	33.4, 22.2	34.2, 22.6	33.3, 22.1	33.3, 22.2
h_{in} - h_{out}, mm	2.5, 8.5	2.6, 8.8	2.6, 8.5	2.8, 8.5

Table 4: Analysis over four RITs with the same SP (0.011 m) and Vr (14) but characterized by different expansion inlet and outlet conditions and compressibility factors. Results are obtained optimizing the turbines with RITML.

quite different, the corresponding specific speed ω_s is similar for all the cases. Moreover, the four turbines exhibit very similar efficiencies that lie in an interval ranging between ±0.65% with respect to the average value of 90.35%. This deviation is within the range of accuracy claimed by the adopted mean line method. This analysis supports the choice of adopting SP and Vr as independent similarity theory parameters for the turbine map definition.

3.3. RIT efficiency sensitivity analysis: effects of operating fluid

The effectiveness of SP and Vr as independent parameters was also tested considering a set of operating fluids. Several turbines were in fact optimized adopting RITML code and imposing the same values of size parameter, volume ratio, and compressibility factor but considering different operating fluids. Particularly, two refrigerants (R1233zd and R134a), a hydrocarbon (cyclopentane), and a siloxane (MM) were selected to span wide ranges of molecular complexity and weight. The optimizations were carried for a fixed inlet compressibility factor Z of 0.63 and for 3 different combinations of SP and Vr (namely SP = 0.007 m and Vr = 5, SP = 0.008 m and Vr = 50, SP = 0.01 and VR = 50). The results of the optimization procedures for SP = 0.008 m

Parameter	R12333zd	R134a	Cyclopentane	MM
T_{in} - p_{in}, °C - bar	255.2, 70	180.2, 85	280.3, 49	286.3, 22
$T_{out,is}$ - p_{out} , °C - bar	119.7, 1.6	31.2, 1.7	162, 1.2	229.4, 0.62
m_{ORC}, g/s	128.2	144.9	66	45.6
Z_{in} - Z_{out}	0.63, 0.98	0.63, 0.97	0.63, 0.98	0.63, 0.99
η_{turb}, %	77.3	76.9	77.4	78
Nozzle				
D_{in} - D_{out}, mm	36.1, 25.1	39.8, 26.6	36.1, 25.1	34.3, 24.3
h_{in} -h_{out}, mm	2.1, 2.1	2.1, 2.1	2.1, 2.1	2.1, 2.1
Rotor				
ω_s - ω, kRPM	0.99, 189	0.96, 187	0.98, 268	1, 185
D_{in} - D_{out}, mm	23.8, 16.9	24.5, 17.3	23.9, 17	23.3, 16.6
h_{in} - h_{out}, mm	2, 4.3	2, 4.6	2, 4.4	2.1, 4.1

Table 5: Analysis over various RITs with the same SP (0.008 m), Vr (50), and Z (0.63) but characterized by different operating fluids. Results are obtained optimizing the turbines with RITML.

and Vr = 50 are summarized in Table 5. Although operated with different fluids, the optimized turbines are characterized by similar non-dimensional parameters and geometric dimensions, all of them being characterized by the same SP, as well as by comparable values of the specific speed ω_s. Moreover, the turbines exhibit very similar efficiencies that lie in an interval ranging between ±0.55% with respect to the average value of 77.45%. The deviation in terms of efficiency is even lower for the other combinations of SP and Vr analyzed, namely ±0.25% for SP = 0.007 m and Vr = 5 and ±0.5% for SP = 0.01 and VR = 50. As pointed out in Section 3.2, these deviations are within the range of accuracy claimed by the adopted mean line method, providing another evidence supporting the choice of SP and Vr as independent parameters for the turbine map definition.

3.4. RIT maximum efficiency map definition

Single-stage radial inflow turbine maximum efficiency map is defined by optimizing 22 different turbines (markers in Figure 2.a) covering most of the region of possible SP and Vr values obtained through the preliminary analysis described in Section 3.1. Figure 2.b depicts the maximum attainable turbine efficiency against the specific speed for the three designs enumerated in Figure 2.a. Additionally, Figure 2.c reports the loss breakdown for six test case optimized turbines, those represented by grey circles in Figure 2.a, whose choice allows to isolate and investigate separately the effects of Vr and SP on the variation of the different loss contributions. The following observations can be reported:

- Turbine SP and Vr strongly affect turbine maximum efficiency which cannot be assumed constant in the whole design space. Calculated values range between 67.1% and 91.9% but lower efficiency is expected for Vr higher than 50 and SP lower than 0.007 m;

- Rotational speed has a large impact on turbine performance and must be carefully optimized. On the contrary, although depending on SP and Vr, the optimal specific speed ranges from 0.9 to 1.04 for most of the optimized turbines, with the exception of 3 of them for which $0.8 < \omega_s < 0.9$. This analysis confirms that a good first attempt value of ω_s is around 1, as also suggested by [14];

- An increment of Vr leads to an efficiency penalization mainly due to an increase of stator passage loss contribution. In fact, higher Vr values lead to lower pressure levels at the nozzle outlet, which in turn imply larger Mach number values and, consequently, higher losses associated with blade boundary layers development. Performance penalization is more marked at smaller SP;

- A reduction of SP produces a pronounced increase of the nozzle passage loss contribution. A possible explanation of this effect is likely to be ascribed to the geometry dimensions reduction that results decreasing the SP value. In fact, the turbine size shrinking is limited by the constraints previously mentioned concerning the minimum values of main geometrical parameters. Therefore, to reach the desired pressure level at the nozzle outlet, mainly affected by the expansion ratio Vr, the optimizer is forced to rise the nozzle outlet angle value, leading an increase of the flow wetted surface and in turn of the friction loss contribution. The increment of clearance losses for lower SP values is to be ascribed to the increase of axial and radial gap relative size occurring when the geometry is shrunk;

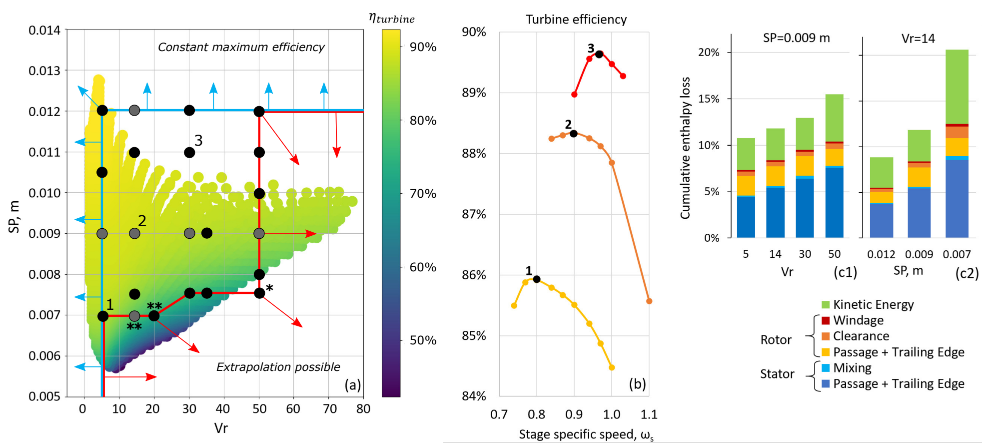

Figure 2: (a) turbine maximum efficiency as function of SP and Vr, markers are the turbines optimized with RITML mean line code. (b) variation of turbine efficiency for markers 1-2-3 as function of turbine ω_s (c) enthalpy loss breakdown for (left) turbines with the same SP (0.009m) and different Vr (5-50) and (right) turbines with same Vr (14) and different SP (0.007m-0.012m).

- To develop the map the rotational speed has not been limited. As result, values of rotational speed around 200000 RPM have been found for turbine labelled with * in Figure 2.a, a strong efficiency penalization is expected for machines in this region if maximum shaft rotational speed is constrained to lower values because of bearings, lubrification and frequency conversion issues.

Computed maximum efficiency values have been interpolated with a best fit correlation having a corrected R^2 equal to 0.993 and average absolute deviation equal to 0.38%, the difference being above 1% only for the 2 turbines labelled with ** in Figure 2.a. The interpolating relation is reported below and the corresponding coefficients A_{ij} are listed in Table 6.

$$\eta_{turb} = \sum_{i=0}^{5} \sum_{j=0}^{2} A_{ij} \ln^i(SP) \ln^j(Vr) \qquad \text{with } i+j \leq 5 \tag{2}$$

Extrapolation of Equation 2 for Vr > 50 and SP < 7 mm is not recommended because it is not supported by any experimental or numerical evidence and can likely result in turbine performance overestimation. On the contrary, for Vr < 5 and SP above 12 mm the efficiency can be kept equal to the efficiency

Coeff.	Value	Coeff.	Value	Coeff.	Value
A_{00}	9103.26	A_{12}	28.10	A_{31}	-60.21
A_{01}	-1512.62	A_{20}	3962.80	A_{32}	0.4798
A_{02}	41.35	A_{21}	-421.09	A_{40}	85.22
A_{10}	9510.39	A_{22}	6.36	A_{41}	-3.22
A_{11}	-1305.07	A_{30}	823.11	A_{50}	3.52

Table 6: Coefficients of interpolating relation for the turbine maximum efficiency performance map.

value obtained at the closer point on the map boundary, which however would result in a slight underestimation of turbine performance according to the very flat trend of the performance map for small Vr and large SP. It is worth to highlight that the value of efficiency obtained through the map is the upper bound achievable from numerical optimization based on mean-line model, which do not consider some possible critical aspects such as detailed shock patterns within the channels, leakage flows, and loss contributions interaction. Therefore, any turbine design must be confirmed with detailed 3D high-fidelity CFD analyses. In addition, the calculated efficiencies strongly depend (especially for small SP and large Vr) on the investigated design variable ranges and constraints adopted. Lower efficiency values can be obtained increasing the lower bound of relevant geometrical features, such as trailing edge thicknesses and clearances, investigating a narrower design space, or limiting rotational speed maximum value because of limits of generator and bearings capabilities.

4. ORC comprehensive design

Once defined, the turbine performance map was implemented in the ORC design tool to assess the effects of a realistic expander efficiency values during the cycle optimization process. For this purpose, two analyses were carried out: the first one focuses on R1233zd(E) and aims to investigate how the turbine performance map affect cycle design variable optimal values while the second one extends the analysis to different working fluids.

4.1. Performance investigation with working fluid R1233zd

Figure 3.a depicts the maximum cycle efficiency map retrieved for the non-recuperative cycle with R1233zd and by adopting the turbine efficiency correlation calibrated in previous section. This map is to be compared against the map of Figure 1.a obtained for a constant turbine efficiency equal to 80% in order to understand the effects on cycle design optimization attainable using realistic values of turbine efficiency rather than assuming a fixed value independently of the cycle thermodynamic and to catch the trade-off between optimizing cycle theoretical performance and the need of maximizing turbine performance. Calculated turbine efficiency is reported in Figure 3.b in function of condensation temperature and cycle maximum pressure. As evidenced by Figure 3.b, adopting high condensation temperature and high maximum pressures would strongly penalize the turbine efficiency due to SP reduction. On the contrary, the lower is the maximum pressure and the condensing temperature the higher is the turbine performance. This behavior of the expander reflects on cycle efficiency, which tend to decrease for high values of p_{max} and T_{cond}, as can be inferred in Figure 3.c, reporting the difference in cycle efficiency between the cases with and without the turbine map. Also the optimal design obtained using the turbine efficiency map (green dot in Figure 3.a) reflects these considerations and selects an optimal turbine inlet pressure (50.59 bar) and a condensation temperature (35 °C) lower than the 80% turbine efficiency case (CASE B in Table 3 and red dot in Figures 1.a and 3.a) in order to improve turbine performance thanks to lower Vr (28.76) and a larger SP (8.54 mm). The difference between the cycle performance calculated with turbine efficiency correlation and the case with fixed turbine efficiency equal to 80% (refer to Figure 1.a) is reported in Figure 3.c. It is interesting to note that in most of the design space the difference is limited to around 1.5%-2% points of efficiency that corresponds to a relative difference of around 10%-15%. Similar observations are valid also for the recuperative cycle. Optimal recuperative and non-recuperative cycle results obtained with turbine efficiency correlation are reported in Table 7.

A final example is also proposed in Table 7 considering also an engine of a smaller size by simply reducing the exhaust mass flow rate down to 0.134 kg/s (-33%), still implementing the turbine efficiency map and considering non-recuperative cycle configuration. If the design point is kept the same obtained with the fixed turbine efficiency assumption the lower organic fluid mass flow rate would result in a lower SP and consequently in a very low realistic turbine efficiency value. In this case the optimization algorithm

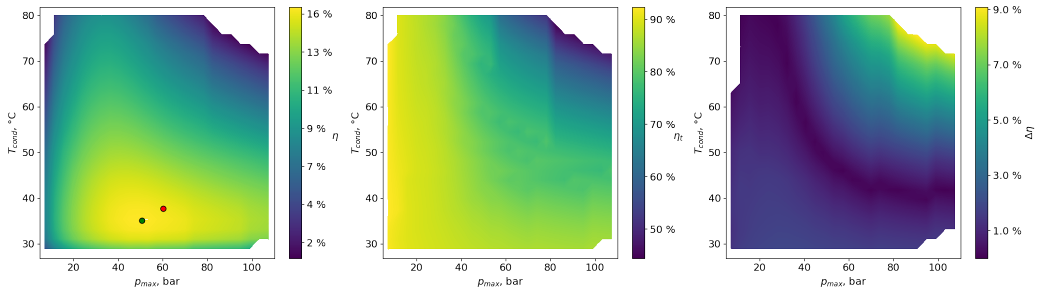

Figure 3: Comprehensive analysis results for the non-recuperative case. (a) cycle efficiency as function of maximum pressure, condensation temperature at optimized turbine inlet temperature, (b) turbine efficiency for the optimal cycles, (c) difference between optimal cycle efficiency adopting turbine performance map vs constant turbine efficiency. Red marker is the optimal design point with 80% constant turbine efficiency while green one corresponds to the ORC optimization with turbine map implemented.

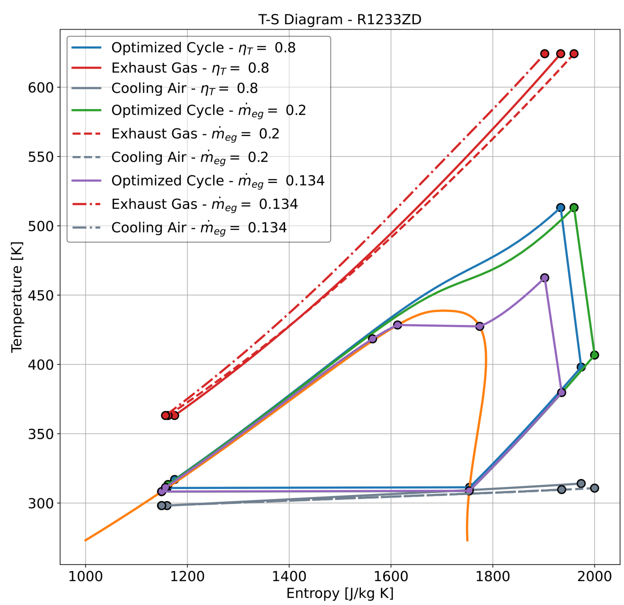

Figure 4: Temperature-specific entropy diagram for: the optimal non recuperative cycle with fixed turbine 80%, the two optimal non recuperative cycles adopting the turbine map with nominal and reduced exhaust mass flow rate.

Case	Non Rec	Rec	Non Rec (-33%)
T_{cond},°C	35.0	34.9	35.1
p_{max}, bar	50.6	54.2	29.5
T_{max}, °C	240	240	189.3
$\Delta T_{pp,rec}$, °C	-	2	-
η_{sys}, %	16.2	19.9	13.7
W_{el}, kW	8.7	10.8	5.0
m_{ORC}, g/s	163.1	198.4	123.0
SP, mm	8.5	9.3	7.6
VR	28.7	31.1	16.2
η_{turb}, %	85.7	87.7	83.6

Table 7: Optimal results for the non-recuperative and the recuperative cycle adopting turbine performance map and results for both normal and reduced size (-33%) engine.

reduces the maximum pressure in order to reduce the turbine enthalpy drop, increasing the turbine SP by concurrently reducing the Vr, and getting the best trade-off between cycle performance and turbine efficiency. Optimal cycle for this reduced size case is subcritical (29.5 bar) and superheated with an optimal turbine inlet temperature considerably lower than the maximum value (189.3°C). Figure 4 compares the temperature-specific entropy ($T-s$) diagrams for the three optimal non recuperative cycles: the one resulting from a constant turbine efficiency (80%), which represents the term of comparison, and the two cycles obtained exploiting the turbine performance map and characterized by exhaust mass flow of 0.2 kg/s and 0.134 kg/s respectively, showing the impact of the adoption of realistic turbine efficiency values on optimal cycle definition. These results show the importance in adopting a turbine efficiency map in the design of small scale ORC based on single stage turbine architecture. In fact, without a proper link between turbine efficiency and cycle parameters (specifically SP and Vr) the cycle optimization always lead to result based on a high pressure ratio supercritical cycle independently of the size of the plant. In case of nominal flue gas mass flow rate this result is rather close to the real optimum obtained implementing the turbine efficiency map while in case of reduced mass flow rate (-33%) this is dramatically wrong and would lead to the adoption of a cycle with an excessive pressure ratio that in turn would cause a non feasible design of the turbine.

4.2. Potential fluid screening - cycle performance assessment

As final analysis, the thermodynamic cycle was optimized by means of the ORC design tool implemented with the turbine efficiency map for a set of potential operating fluids. In particular, the list of fluids chosen includes 5 hydrocarbons (n-Pentane, cyclopentane, hexane, cyclohexane, Toluene), 4 refrigerants (R134a, R1233zd, R1234yf, R245fa), and 2 siloxanes (MM,MDM). The set aims at including most of state-of-the-art ORC working fluids, still bewaring of current environmental and safety regulations, and concurrently at investigating wide ranges of compound molecular complexity, critical point and molecular weight.

The non-recuperative cycle configuration was optimized for each operating fluid above mentioned, exploiting as design variables the three parameters reported in Section 3.1, namely P_{max}, T_{cond}, and T_{max}. Most relevant constraints applied to the optimization process concern the avoidance of two-phase flow through the expander, a maximum Vr equal to 60 to avoid unfeasible single-stage turbine geometries and excessively large nozzle outlet Mach numbers, and minimum condensing pressure equal to 0.1 bar to avoid inward leakage issues. The optimizations were carried out for four different cases: CASE R is the reference case and adopts a fixed turbine efficiency (85%); the results are independent of the engine size, CASE S, M and L implement turbine efficiency map and different engine sizes equal to $\dot{m}_{eg} = 0.1$ kg/s, $\dot{m}_{eg} = 0.2$ kg/s, and $\dot{m}_{eg} = 0.4$ kg/s respectively. The results of this analysis are summarized in Table 8, in which the plant efficiency values are sorted for the 4 cases investigated, and in Figure 5, which depicts the optimal thermodynamic cycles for cyclopentane and R1234yf for cases S, M and L.

Comparing CASE S, M and L it is possible to appreciate the impact of using turbine performance map on the cycle definition and performance, depending on the working fluid and plant size. Fluids characterized by high critical temperature and high molar mass (cyclopentane, hexane, toluene) can attain good turbine efficiency also for small scale systems thanks to the combined effect of low condensing pressures and low specific enthalpy drop, which result in high SP values. Increasing the size for these fluids is beneficial but the gain in performance is rather limited. However, as evidenced in Figure 5.a, the cycle configuration for cyclopentane changes varying the engine size. In particular, for CASE M and L the cycle adopts very high evaporation pressure close to the critical one, saturating the constraint on maximum turbine volume ratio (60), and the cycle architecture and turbine efficiency (about 89%) are rather independent on the size. On the contrary, for CASE S the cycle adopts a lower evaporation and maximum temperatures thus leading to lower volume ratio (39.6) and enthalpy drop in order to limit the reduction of SP and get good turbine performance also in this case of smaller engine size.

These effects are much more pronounced for low critical temperature and low molecular weight fluids that are characterized by higher condensation pressure and thus by lower volumetric flow rates, leading to low values of SP and consequently to miniaturized machines that suffer of low efficiencies. Considering R1234yf (Figure 5.b), the optimal cycle changes dramatically for the different cases. For CASE L the high working fluid mass flow rate allows to have reasonable SP also in case of supercritical cycles. On the contrary, reducing the engine size the optimal cycle moves towards subcritical configurations, becoming a nearly saturated cycle at very low evaporation temperature for CASE S. In this latter case the optimization algorithm pushes the condensing temperature close to the minimum one in order to increase the volumetric flow rate at turbine outlet, and reduces both the maximum temperature and pressure in order to reduce the turbine enthalpy drop leading to reasonable SP. The final cycle in CASE S has an extremely low efficiency (about 1%), due to the combination of very small pressure ratios and a penalized turbine efficiency (69.9%). However, this result is compliant with the use of a single stage radial inflow turbine and it is remarkably different from the result attainable in CASE R (fixed turbine efficiency) that adopts a supercritical cycle with a combination of very low SP (4.5 mm) and moderate Vr (10.6), which are non-compatible with the selected turbine architecture and that in turn would result in an unfeasible turbine design. A final consideration can be highlighted for R1233zd(e), the fluid already selected as a promising candidate for this application. If no map of turbine efficiency is adopted (CASE R) R1233zd(e) is certainly not the most promising fluid ranking in 6th position with an efficiency gap of around 4 points with respect to the best fluid (16.22% vs 20.15%). This positioning however is not representative of the potential this fluid; in fact, if turbine efficiency dependency on cycle parameters is accounted for the results are radically different. In CASE S, the small engine size produces a penalization of turbine efficiency which in turn leads to a subcritical cycle with strongly penalized efficiency (11.7%) which is 9 points of efficiency lower than the one associated with the best fluid. Increasing the engine size (CASE M and CASE L) the performance of R1233zd increases remarkably, approaching the the best fluid (cyclopentane) efficiency in the larger size case (20.73% vs 21.34%) mak-

CASE R Constant η_{turb}		CASE S $\dot{m}_{eg} = 0.1$ kg/s		CASE M $\dot{m}_{eg} = 0.2$ kg/s		CASE L $\dot{m}_{eg} = 0.4$ kg/s	
Fluid	η_{sys}, %	Fluid	η_{sys}, %	Fluid	η_{sys}, %	Fluid	η_{sys}, %
Cyclopen	20.15	Toluene	20.61	Cyclopen	20.96	Cyclopen	21.43
Toluene	19.44	Cyclohex	20.17	Toluene	20.63	R1233zd	20.73
Cyclohex	19.04	Cyclopen	17.86	Cyclohex	20.18	Toluene	20.61
Pentane	17.01	Hexane	17.45	Hexane	17.84	Cyclohex	20.19
Hexane	16.79	MM	14.73	Pentane	16.67	Pentane	18.08
R1233zd	16.22	Pentane	13.29	R1233zd	16.17	Hexane	17.84
R245fa	16.15	R1233zd	11.69	MM	14.65	R245fa	16.90
R134a	14.23	MDM	11.51	R245fa	14.05	MM	14.72
MM	13.85	R245fa	9.90	MDM	11.47	MDM	11.47
R1234yf	11.37	R1234yf	1.31	R1234yf	6.09	R134a	10.97
MDM	10.81	R134a	0.79	R134a	5.68	R1234yf	10.13

Table 8: Sorted optimal plant efficiencies for the whole set of potential working fluids and for the four cases investigated.

ing it a very attractive option considering the lower flammability risk with respect to hydrocarbons.

5. Conclusions

Main outcomes of this work are related to demonstrate the importance of adopting reliable efficiency maps for turbomachinery especially in those applications, like on board waste heat recovery, where single stage radial inflow architecture are adopted and turbine number of stages cannot be varied to keep efficiency stable independently of the volume ratio. It is possible to underline that the implementation of a map for expected turbine performance allows to guide the optimization algorithm towards solution which are more representative of the correct optimal design of the system. The results show that the adoption of a fixed turbine efficiency can be very misleading in terms of optimal cycle definition and selection of the optimal fluids. In particular, for low critical temperature fluids (mainly refrigerants) the use of constant turbine efficiency can lead to a large overestimation of their potential in small scale applications where they are not recommended and to exclude them for WHR from large engines where on the contrary they can get (especially R1233zde) very competitive performance with respect to hydrocarbons. Finally, it is possible to underline that the use of constant turbine

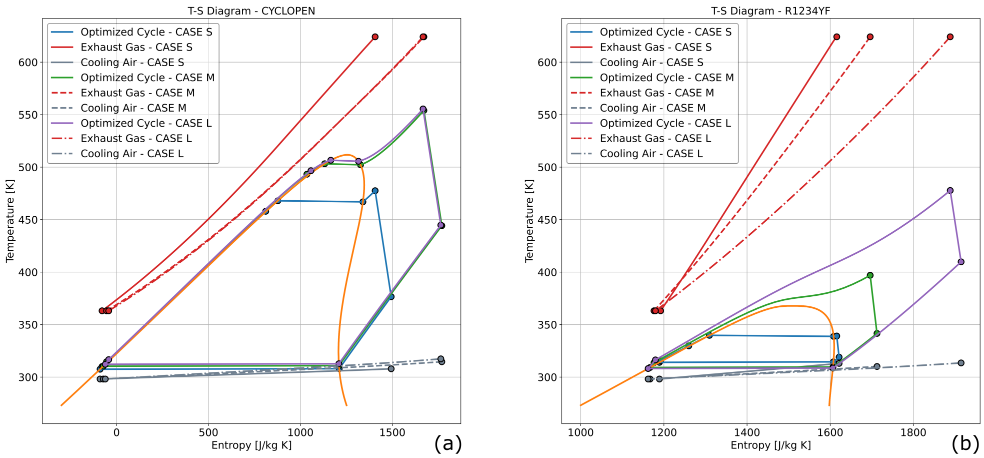

Figure 5: Temperature-specific entropy diagram of optimal non recuperative cycles implementing the turbine performance map with 3 different exhaust mass flow rate values for: (a) Cyclopentane, (b) R1234yf.

efficiency assumption for these fluids results in optimal solutions that may strongly affect the final feasibility of the power plant. In fact, such approach may lead to select a cycle thermodynamic not compatible with the effective usage of a single stage radial inflow turbine.

This result has been obtained thanks to an extensive numerical activity on turbine geometry optimization for a large range of SP and Vr selected as independent parameters. This activity allows to define a performance map that can be used with sufficient accuracy ($\pm 1\%$, as demonstrated in Section 3.2, plus the intrinsic prediction uncertainty of the mean-line model), independently of the specific value of pressure ratio, inlet compressibility factor, and the adopted working fluid. The fitted equation can be thus adopted as a very general fluid-independent turbine performance map representing the maximum efficiency attainable with an optimization of both blade geometry and rotational speed for single stage radial inflow turbine architecture. Turbine performance reduces for increasing Vr and reducing SP values. The former efficiency drop is due to the presence of highly supersonic flows at the nozzle outlet and the need of adopting very large blade span variation within the rotor. On the contrary, reduced SP values lead to small turbine sizes and to the consequent increase of loss contributions related to those geometrical features that cannot be freely scaled down, such as clearances and trailing edge thicknesses. Additionally, turbine shrinking to comply with a SP reduction cannot be always achieved due to the physical constraints considered to ensure the mechanical feasibility of the final proposed geometry. In particular, for Vr over 60 and SP below 7 mm is difficult to get a feasible turbine design because of the limit of subsonic relative flow at the rotor inlet, the increase of profile and secondary losses, and the reduced physical dimensions of the machine.

The performance map can be easily integrated in numerical models for cycle optimization and allows to create a direct link between expander efficiency and cycle design parameters, leading to the definition of optimal cycles that do not result in an unfeasible turbine design.

Acknowledgement

The authors would like to tank the department of Excellence since this research is part of the Energy for Motion project of the Department of Energy of Politecnico di Milano, funded by the Italian Ministry of University and Research (MUR) through the Department of Excellence grant 2018-2022.

References

[1] T. Tartière, M. Astolfi, A world overview of the organic rankine cycle market, Energy Procedia 129 (2017) 2–9.

[2] C. Yang, Y. Li, Fuel-saving performance and main losses of an organic-rankine-cycle-based exhaust heat recovery system in heavy truck application scenarios, Applied Thermal Engineering 193 (2021) 117025.

[3] V. Dolz, R. Novella, A. García, J. Sánchez, Hd diesel engine equipped with a bottoming rankine cycle as a waste heat recovery system. part 1: Study and analysis of the waste heat energy, Applied Thermal Engineering 36 (2012) 269–278.

[4] X. Wu, J. Chen, L. Xie, Optimal design of organic rankine cycles for exhaust heat recovery from light-duty vehicles in view of various exhaust gas conditions and negative aspects of mobile vehicles, Applied Thermal Engineering 179 (2020) 115645.

[5] S. Amicabile, J.-I. Lee, D. Kum, A comprehensive design methodology of organic rankine cycles for the waste heat recovery of automotive heavy-duty diesel engines, Applied Thermal Engineering 87 (2015) 574–585.

[6] C. Sprouse III, C. Depcik, Review of organic rankine cycles for internal combustion engine exhaust waste heat recovery, Applied thermal engineering 51 (2013) 711–722.

[7] P. Colonna, E. Casati, C. Trapp, T. Mathijssen, J. Larjola, T. Turunen-Saaresti, A. Uusitalo, Organic Rankine Cycle Power Systems: From the Concept to Current Technology, Applications, and an Outlook to the Future, Journal of Engineering for Gas Turbines and Power 137 (2015). doi:10.1115/1.4029884.

[8] J. Rijpkema, S. Thantla, J. Fridh, S. B. Andersson, K. Munch, Experimental investigation and modeling of a reciprocating piston expander for waste heat recovery from a truck engine, Applied Thermal Engineering 186 (2021) 116425.

[9] G. Persico, M. Pini, Fluid dynamic design of organic rankine cycle turbines, in: Organic Rankine Cycle (ORC) Power Systems, Elsevier, 2017, pp. 253–297. doi:10.1016/b978-0-08-100510-1.00008-9.

[10] M. Glensvig, H. Schreier, M. Tizianel, H. Theissl, P. Krähenbühl, F. Cococcetta, I. Calaon, Testing of a long haul demonstrator vehicle with a waste heat recovery system on public road, Technical Report, SAE Technical Paper, 2016.

[11] A. Bademlioglu, A. Canbolat, N. Yamankaradeniz, O. Kaynakli, Investigation of parameters affecting organic rankine cycle efficiency by using taguchi and anova methods, Applied Thermal Engineering 145 (2018) 221–228.

[12] A. Meroni, J. G. Andreasen, G. Persico, F. Haglind, Optimization of organic rankine cycle power systems considering multistage axial turbine design, Applied Energy 209 (2018) 339–354.

[13] S. Bahamonde, M. Pini, C. De Servi, A. Rubino, P. Colonna, Method for the preliminary fluid dynamic design of high-temperature mini-organic rankine cycle turbines, Journal of Engineering for Gas Turbines and Power 139 (2017).

[14] A. Perdichizzi, G. Lozza, Design criteria and efficiency prediction for radial inflow turbines, in: ASME 1987 International Gas Turbine Confer-

ence and Exhibition, American Society of Mechanical Engineers Digital Collection, 1987.

[15] M. Astolfi, E. Macchi, Efficiency correlations for axial flow turbines working with non-conventional fluids, in: 3rd International Seminar on ORC Power Systems, 2015, pp. 12–14.

[16] L. Da Lio, G. Manente, A. Lazzaretto, A mean-line model to predict the design efficiency of radial inflow turbines in organic rankine cycle (orc) systems, Applied Energy 205 (2017) 187–209.

[17] M. T. White, A. I. Sayma, Simultaneous cycle optimization and fluid selection for orc systems accounting for the effect of the operating conditions on turbine efficiency, Frontiers in Energy Research 7 (2019) 50.

[18] A. P. E. Macchi, Efficiency prediction for axial flow turbines operating with non-conventional working fluids, J. of Eng. for Power 103 (1981) 712–724.

[19] M. Masi, L. Da Lio, A. Lazzaretto, An insight into the similarity approach to predict the maximum efficiency of organic rankine cycle turbines, Energy 198 (2020) 117278.

[20] M. Manfredi, M. Alberio, M. Astolfi, A. Spinelli, A reduced-order model for the preliminary design of small-scale radial inflow turbines, in: Still to be published, ????

[21] I. H. Bell, J. Wronski, S. Quoilin, V. Lemort, Pure and pseudo-pure fluid thermophysical property evaluation and the open-source thermophysical property library coolprop, Industrial & Engineering Chemistry Research 53 (2014) 2498–2508. doi:10.1021/ie4033999. arXiv:http://pubs.acs.org/doi/pdf/10.1021/ie4033999.

[22] E. W. Lemmon, , I. H. Bell, M. L. Huber, M. O. McLinden, NIST Standard Reference Database 23: Reference Fluid Thermodynamic and Transport Properties-REFPROP, Version 10.0, National Institute of Standards and Technology, 2018. URL: https://www.nist.gov/srd/refprop. doi:https://doi.org/10.18434/T4/1502528.

[23] K. Yang, M. Bargende, M. Grill, Evaluation of Engine-Related Restrictions for the Global Efficiency by Using a Rankine Cycle-Based Waste Heat Recovery System on Heavy Duty Truck by Means of 1D-Simulation, Technical Report, SAE Technical Paper, 2018.

[24] M. Astolfi, E. Martelli, L. Pierobon, Thermodynamic and technoeconomic optimization of organic rankine cycle systems, in: Organic Rankine cycle (ORC) power systems, Elsevier, 2017, pp. 173–249.

[25] M. Manfredi, M. Alberio, M. Astolfi, A. Spinelli, A reduced-order model for the preliminary design of small-scale radial inflow turbines, in: Turbo Expo: Power for Land, Sea, and Air, volume 84966, American Society of Mechanical Engineers, 2021, p. V004T06A013.

[26] E. F. T. Committee, Hcfo-1233zd(e) chillers receive environment awards around the world, http://precog.iiitd.edu.in/people/anupama, 2020.

Highlights

Definition of a general performance map for single stage radial inflow turbines and analysis of the impact of expander performance on the optimal ORC design in on-board waste heat recovery applications.

Marco Manfredi, Andrea Spinelli, Marco Astolfi

- We define a general performance map for ORC single stage radial inflow turbines
- Effect of Vr and SP on turbine efficiency is discussed with a detailed loss analysis
- We integrated the turbine performance map in the ORC optimization routine
- The use of turbine performance map can greatly affect optimal cycle definition
- The use of turbine performance map strongly affects the choice of the optimal fluid